International Journal of
Water and Wastewater Treatment
ISSN 2381-5299 | Open Access

RESEARCH ARTICLE

Volume 6 - Issue 3

Kaolinite Detachment from Silica Substrate - Laboratory and Theoretical Study

Yang Y, Dang-Le B, Kutty G, Mbeveri S, Carageorgos T, Badalyan A, Bedrikovetsky P*

Australian School of Petroleum and Energy Resources, University of Adelaide, North Terrace, Australia

***Corresponding author:** Bedrikovetsky P, Australian School of Petroleum and Energy Resources, University of Adelaide, North Terrace, Frome Road gate 6, SA 5005, Australia, E-mail: pavel.bedrikovetski@adelaide.edu.au

Received: 07 Nov, 2020 | **Accepted:** 17 Nov, 2020 | **Published:** 24 Nov, 2020

Citation: Yang Y, Dang-Le B, Kutty G, Mbeveri S, Carageorgos T, et al. (2020) Kaolinite Detachment from Silica Substrate - Laboratory and Theoretical Study. Int J Water Wastewater Treat 6(3): dx.doi.org/10.16966/2381-5299.174

Abstract

The paper presents laboratory study of kaolinite fines detachment from silica/glass substrate in the visualisation cell, which mimics clay release during colloidal and suspension flows in aquifers. The cell saturation by particles is performed until full stabilization during the attachment process; further, detachment of particles occurs during piecewise-constant increasing of flow velocity. The detachment data calculated from microscope images are compared with the forces and torques detaching the particles. Qualitative agreement between the modelling and laboratory data is observed.

Keywords: Colloid; Suspension; Particle detachment; Mechanical equilibrium; Detachment modelling; Laboratory study; Visualization; Colloidal transport; Porous media

Introduction

Kaolinite detachment from rock surface of natural reservoir sandstones occurs in numerous natural and technological processes [1-3]. The incomplete list includes colloidal-suspension transport in subterranean waters, wastewater treatment, fresh water storage in aquifers, brine exchange between aquifers and ocean, transport of bacteria, virus, and contaminants with an adsorption on kaolinite, enhanced geothermal projects with cold water injection and steam / hot water production, high-rate production of viscous oils and water injection in oilfields [4-8]. Therefore, detachment of kaolinite from rock surfaces with further migration has been studied in many works and is a topic of current on-going research [9-11].

Mathematical model for phase suspension colloidal transport with particle detachment have been developed in numerous works [12-16]. Several exact solutions have been derived, yielding simple analytical models for planning, design, and data treatment of laboratory core floods [17-21].

Particles from the colloidal-suspension flux are captured by the rock due to size exclusion, straining, attachment, diffusion into dead-end pores, and gravitational segregation [22]. In the current paper, we discuss attachment of particles by electrostatic forces. The attached particles in the moving fluid are subject to drag, electrostatic, lift and gravitational forces [22,23] (Figure 1). Drag and lift detach the particles, while electrostatic and gravitational forces attach them. The electrostatic force and energy consist of Van der Waals, double-electric layer, and Born components (Figure 2). Numerous laboratory studies present fines detachment in visualisation cells and validate the mechanical-equilibrium detachment criteria [5-8,12]. A recent paper [24] presents a systematic study of attached particle lifting in visualisation cell under changing velocity, salinity, and pH. The work introduced phase diagrams, which allow indicating detachment regions for given temperature, velocity, salinity, and pH. The study has been performed using latex particles attached to glass/silica substrate.

The fine particles in natural colloidal suspension in the above-mentioned processes are clays and silica. The most wide-spread natural fines are kaolinite clays. Several papers study specifically kaolinite transport in porous media [1-3,9-11]. However, laboratory visualisation study for kaolinite detachment and transport is not available.

The current paper fills the gap. We investigate the detachment of kaolinite fines from silica substrate under varying velocities, salinities, and pH values. The observed gradual detachment of fines is attributed to different sizes of kaolinite particles. Calculation of mechanical equilibrium conditions for a medium particle size qualitatively agrees with the detachment observations from the laboratory visualisation tests.

Materials and Methods

This section describes particles, substrate, brine, laboratory setup, and the methodology of laboratory investigation. More detailed description can be found from work [24].

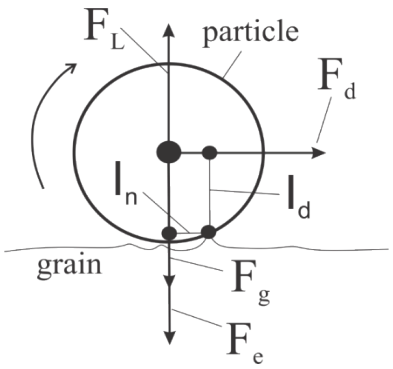

Figure 1: Torque balance criterium for fines detachment: the torques of detaching drag and lift must exceed the torques of attaching electrostatic and gravitational forces.

Substrate, brine, fine particles

The solid substrate is the glass cover slip (Ibidi, Martinsried, Germany). The solid substrate was cleaned by soaking in acetone with further rinsing with ethanol and de-ionized water. Further, the glass substrate was dried for 48 hours at room conditions.

The brine was prepared by dissolution of sodium chloride in DI water. Brine with pH 3 was used for Test 1 and with pH 9 for Test 2. Salinity of 0.3M was used in Test 1, and of 0.1M - in Test 2.

The particles are kaolinite with sizes changing from 0.5 μm to 3.0 μm (Fluka Analytical Pty. Germany).

Experimental setup

The schematic for experimental setup with all major equipment is shown in figure 3. The brine is injected into a visualization cell using an electronic syringe pump. The photos of attached particles in the visualization cell are taken using the optical microscope equipped with a camera. The photos are processed by image treatment software Image J.

Experimental methodology

Initially, the visualization cell was filled with brine. Then the colloidal clay particles with a concentration of 300 ppm were injected into the visualization cell. The lowest linear velocity of E-5 m/s was used to favor fines attachment to solid substrate. After injection of 1.5 cell volumes (PVs), the flow was stopped, and the cell with colloid were left for 24 hours, to reach a stable particle layer of particles attached to the glass substrate. Taken periodically, images allowed controlling the attached particles stabilization (Figures 4,5). This initial state of the attached fully saturated particulate system is called step 0.

The steps 1, 2…10 correspond to increasing piece-wise constant velocities. The velocities in Test 1 were 2.94E-2 m/s, 3.34E-2, 3.38E-2, 4.46E-2, 5.34E-2, 6.53E-2, 8.29E-2, 1.12E-1, 1.63E-1, 2.78E-1, and 7.13e-1m/s for stages 1, 2…10, respectively. The velocities from Test 2 were 2.66E-2m/s, 3.1E-2, 3.72E-2, 4.66E-2, 6.25E-2, 9.47E-2, 1.93E-1, 2.27E-1, 3.32E-1, and to 3.9e-1 m/s for stages 1, 2…10.

The images in figures 4 and 5 present the stabilized conditions, where flux does not detach particles from the glass surface anymore.

Test 1 uses the following conditions: salinity is 0.3M, pH is 3. In test 2, salinity is 0.1M, and pH is 9.

Theory

It is assumed that at the moment of detachment, a particle rotates around the asperity, or the neighboring particle, or the contact point particle-substrate. Figure 1 shows the lever arms for drag (l_d) and l_n for normal force, which is equal to $F_e+F_g-F_l$, where F_e, F_g, and F_l are the electrostatic, gravity, and lift, respectively. The conditions of particle detachment, currently used for prediction of fines lifting and mobilization are [5-7,11-14]: - detaching torques of drag and lift exceed attaching torques of electrostatic and gravitational forces.

$$\left(F_e+F_g\right)l_n < F_d l_d + F_l l_n \qquad (1)$$

-drag exceeds friction force caused by the normal force with Coulomb friction coefficient μ

$$\left(F_e+F_g-F_l\right)\mu < F_d \qquad (2)$$

-lift exceeds the total of electrostatic and gravity forces

$$F_e+F_g < F_l \qquad (3)$$

Fulfillment of detachment condition 1, 2, and 3 results in particle rolling over the surface, particle sliding along the surface, and particle lifting from the surface, respectively.

Figure 2 presents the electrostatic energy profile *versus* separation distance h between the particle and surface. The electrostatic force is equal to minus gradient of the energy:

$$F_e = -\frac{\partial V}{\partial h} \qquad (4)$$

The electrostatic force/energy is the total of Van der Waals, double electrical layer and Born repulsion components. Figure 2a presents the case of favorable attachment where the total energy potential has one minimum; this case corresponds to Test 1. Energy minimum corresponds to vanishing of electrostatic force:

$$F_e\left(h_{\min}\right) = -\frac{\partial V}{\partial h}\left(h_{\min}\right) = 0,\ \frac{\partial F_e}{\partial h}\left(h_{\min}\right) = -\frac{\partial^2 V}{\partial h^2}\left(h_{\min}\right) > 0 \qquad (5)$$

The energy profile V(h) in the interval from h_m to infinity has S-shape. Therefore, there does exist such a separation distance h_{max} which corresponds to maximum electrostatic force.

The case of unfavorable attachment conditions, where the energy potential has two minima is shown in figure 2b; this case corresponds to Test 2.

The electrostatic force Fe in equations 1, 2, and 3 corresponds to maximum value of this force, where the corresponding separation distance h=hm is in inflection point of the energy profile V(h) (Figure 2a):

$$\frac{\partial F_e}{\partial h}\left(h_m\right) = -\frac{\partial^2 V}{\partial h^2}\left(h_m\right) = 0,\ \frac{\partial^2 F_e}{\partial h^2}\left(h_m\right) = -\frac{\partial^3 V}{\partial h^3}\left(h_m\right) < 0,\ h_m > h_{\min} \qquad (6)$$

For unfavorable attachment conditions, the inflection points corresponding to maximum electrostatic forces are located to the right of the corresponding points of energy minima.

Figures 6 and 7 present normalized torques, and the totals of normalized horizontal and vertical forces. The negative values correspond to particle detachment. Here all four forces have been calculated using the formulae presented in works [13,14,24,25].

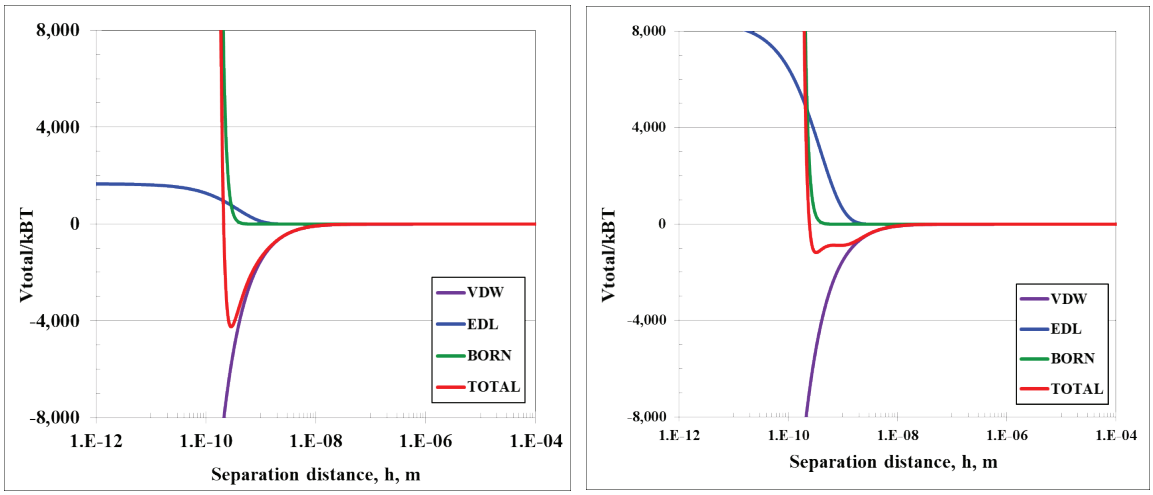

Figure 2: DLVO energy profiles for substrate-particle interaction, a) Favourable conditions for attachment in Test 1; b) Unfavorable conditions for attachment in Test 2.

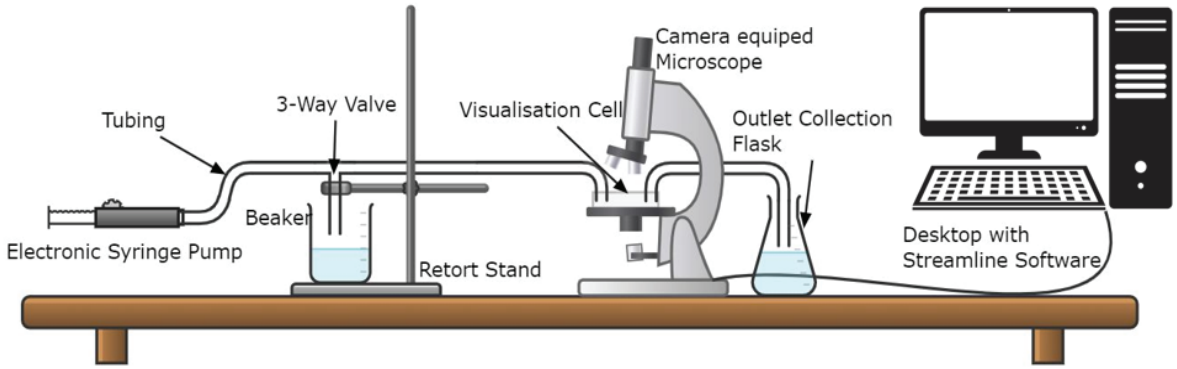

Figure 3: Schematic of laboratory set-up for fines detachment.

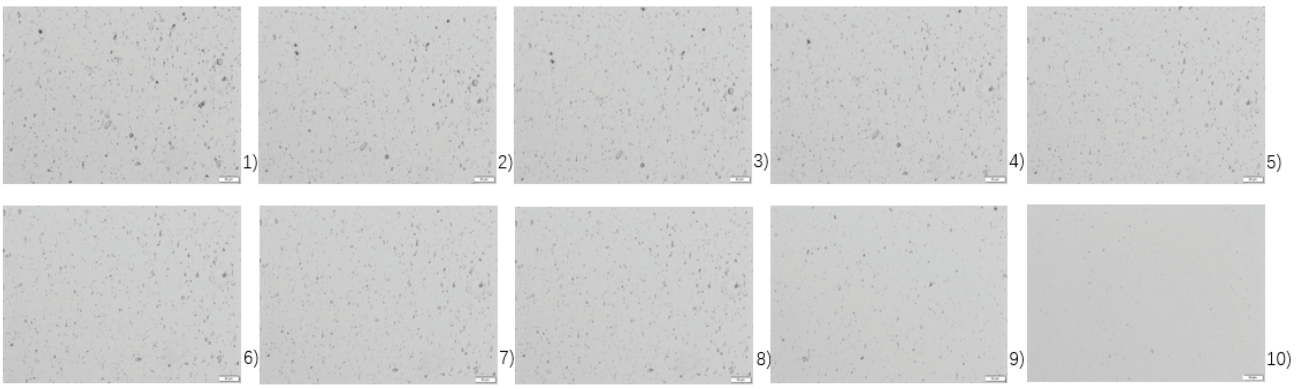

Figure 4: Images of attached particles in Test 1 (steps 1 to 10).

The total electrostatic force $F_e(h)$ is calculated as a total of van der Waals, Double Electric Layer and Born forces [22,23]. The formulae for energy *versus* separation distance h are shown in figures 3a and 3b for Tests 1 and 2, respectively. The h-dependency for van der Waals, Double Electric Layer and Born profiles are shown by the purple, blue, and green curves, respectively. The red curves correspond to the overall energy profile V(h). The calculations show that attachment in Test 1 occurs in favorable conditions, i.e. the energy profile has one (primary) minimum.

The value h_m corresponds to separation distance in immobile fluid. Application of velocity in equation (1) corresponds to the movement of separation distance from h_m to the right, where h is determined by the torque balance equations (1). The increase in velocity and, consequently in drag, yields the increase of electrostatic attraction $F_e(h)$. Particle detachment occurs when the electrostatic force, equilibrating the detached torque reaches the value F_{max}, i.e. the separation distance reaches the value of h_{max}. In the laboratory tests performed, particle size in the injected colloid varies in some limits. Consequently, maximum of electrostatic force varies too, which results in gradual particle detachment.

Figure 2b presents energy profile for conditions of Test 2. The attachment conditions are unfavorable - the energy profile has two minima. The primary minimum is deep, the secondary minimum is shallow. During particle detachment of the saturation stage of the test, some particles settle in primary minimum and some in secondary minimum. Equation 1 of mechanical equilibrium is applied for disjoining distances $h=h_1$ and $h=h_2$ separately. In the immobile fluid, the separation distances h_{1m} and h_{2m} correspond to energy minima. Application of velocity moves h_1 and h_2 to the right from the points h_{1m} and h_{2m}, respectively. The drag, lift and gravity exerting the particles in primary and secondary minima are the same. The lever arms are significantly higher than the separation distances and are also equal in primary and secondary minima. Consequently, the electrostatic forces equilibrating the detaching torques are the same for the particles attached in both minima. Therefore, the tangents of energy profiles in the points h_1 and h_2 are equal.

Secondary minimum is shallow if compared with the primary minimum. Therefore, maximum electrostatic force in secondary minimum is lower than that in primary minimum. Consequently, at some velocity the maximum value of electrostatic force F_{2max} will be reached for particles attached in the secondary minimum, while the electrostatic force in primary minimum is below its maximum value. Therefore, during the tests with sequential increase of the flow velocity, first are detached particles from secondary minimum, and then- from the primary minimum. Maximum electrostatic force for primary minimum is significantly higher than that in secondary minimum, so flow velocity detaching particles from secondary minimum is significantly higher than that for primary minimum.

Results and Discussion

The images of attached particles in Test 1 during the ten stages of Test are given in figure 4. Figure 5 shows the images from Test 2. The main observation is the gradual detachment of particles during increase of the velocities. The particle sizes vary in the interval from 0.5 to 3.0 microns. Yet the forces and torques in equations 1 to 3 correspond median particle radius of 0.7 microns.

Now let us compare these results with the data on mathematical modelling of particle detachment. Figures 6 and 7 present the results of calculations of normalized torque, normalized horizontal force, and normalized vertical force for Tests 1 and 2, respectively. The blue curves correspond to percentage of mobilized particles which grows from 0 at initial stage to almost hundred percent at the tenth stage in figure 6. In figure 7, the percentage of mobilized particles varies from 0 to 60 percent.

Figures 6a and 7a present normalized torque for all steps for lever arm ratio that equals 100, which is a typical value presented in the literature [26-28]. The detachment of particles by rolling starts at the step where the normalized torque becomes negative, which is step 5 for Test 1 and step 7 in figure 7. In both cases, the number of detached particles constitutes a significant fraction of initially attached particles. Figures 6b and 7b correspond to normalized horizontal force; the calculations have been performed for Coulomb fraction coefficient $\mu=0.2$. The particles start detaching when the horizontal force becomes negative, which is step 9 in figure 6b; the detachment of significant amount of particles occurred where the horizontal force changed its signs. In figure 7b, the detachment also occurred during step 9, and also significant fraction of attached particles have been detached.

Normalized vertical force in figure 6c remains positive, i.e. lift does not detach particles attached in primary minimum in favorable case. However, in figure 7, vertical force does detach particles after step

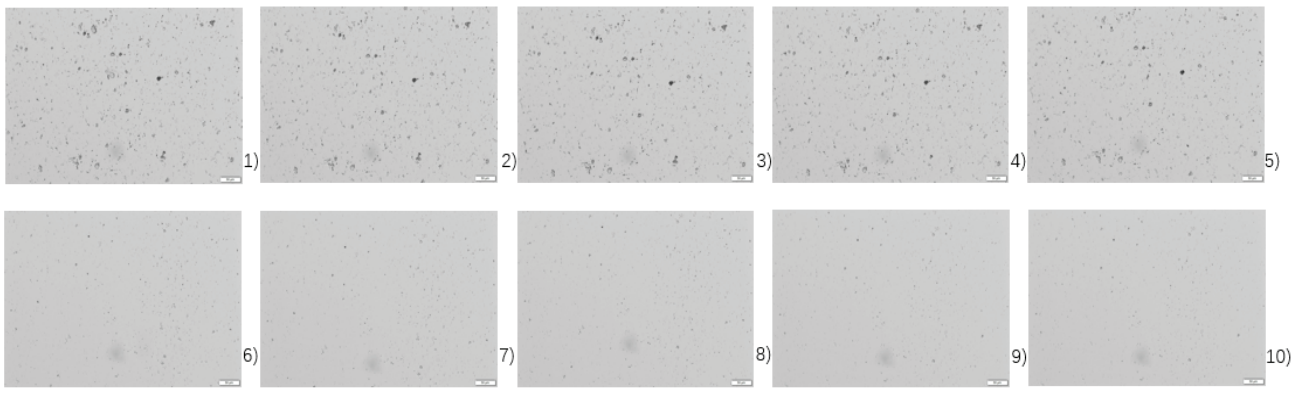

Figure 5: Images of attached particles in Test 2 (steps 1 to 10).

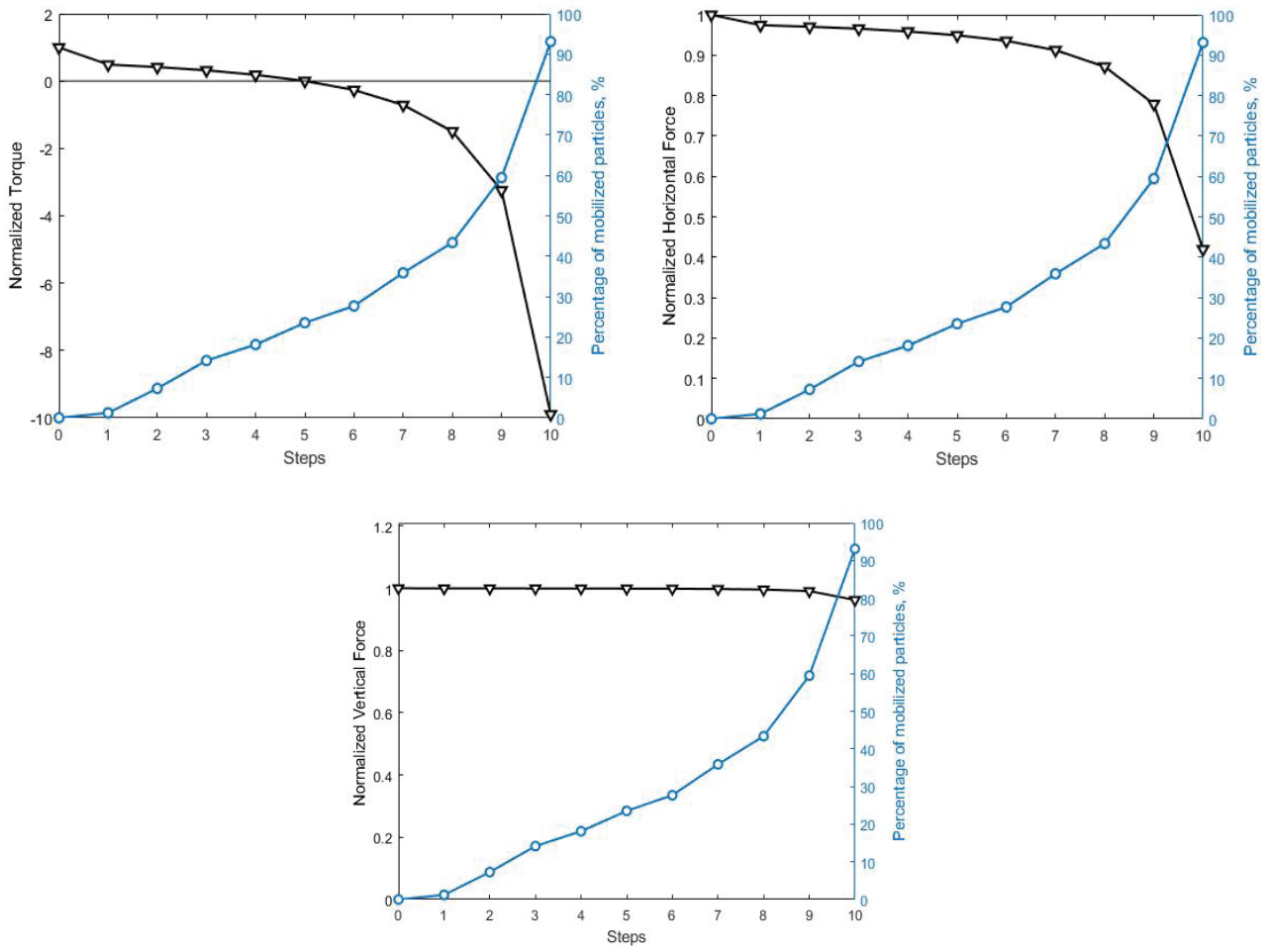

Figure 6: Condition of mechanical equilibrium for favourable attachment (Test 1): a) Normalised rolling torque; b) Normalised horiztonal force; c) Normalised vertical force.

6. The detached particles have been attached in secondary shallow minimum.

To summarize, we performed two flow tests in visualization cell without changing the brine composition and under piece-wise constant increasing flow velocity. We observed gradual detachment of particles during the flow velocity increase. The mechanical equilibrium of particles has been applied for each step (velocity) in the tests. It was observed that the detachment criteria as applied to the average particle size, correspond to detachment of a significant part of the particles.

The formulae for forces applied in equations (1-3) are valid for spherical particles, while the kaolinite particles can be approximated by either cylinders or ellipsoids. The corresponding formulae for either flat cylinders or ellipsoids that are valid for natural kaolinite clays can be obtained by Computational Fluid Dynamics (CFD). This study is out of the scope of the current work.

Distribution of particles over radius yields distribution of forces in the detachment conditions [1-3]. The gradual detachment curves in figures 6 and 7, under known particle size distribution, can be used in order to determine asperity distribution over the substrate surface, like it was done in work [24]. This is also the next step of the research.

The calculation of torques and forces, based on spherical particles with the average size, do not aim to match the detachment blue curves in figures 6 and 7. The goal of the calculations is to find out whether or not particle detachment occurs at the typical values, given by criteria 1, 2, and 3. Indeed, the comparison between the detached concentration curve and the mechanical equilibrium conditions yields the detachment of significant fraction of attached particles. It allows for qualitative explanation of kaolinite particle detachment by the mechanical equilibrium criteria. We expect that, accounting for particle size distribution and kaolinite shape and using more sophisticated mathematical models (like those presented in works [29-32]) would match the detachment concentration curves with high accuracy.

Conclusions

The laboratory study on visualization of particle detachment from solid substrate and its mathematical modelling based on mechanical equilibrium of the attached particles allow drawing the following conclusions.

During the piece-wise constant velocity increase, the particle in our tests detach gradually, while equation (1) suggests simultaneous detachment of all mono-sized particles attached to an ideal plane

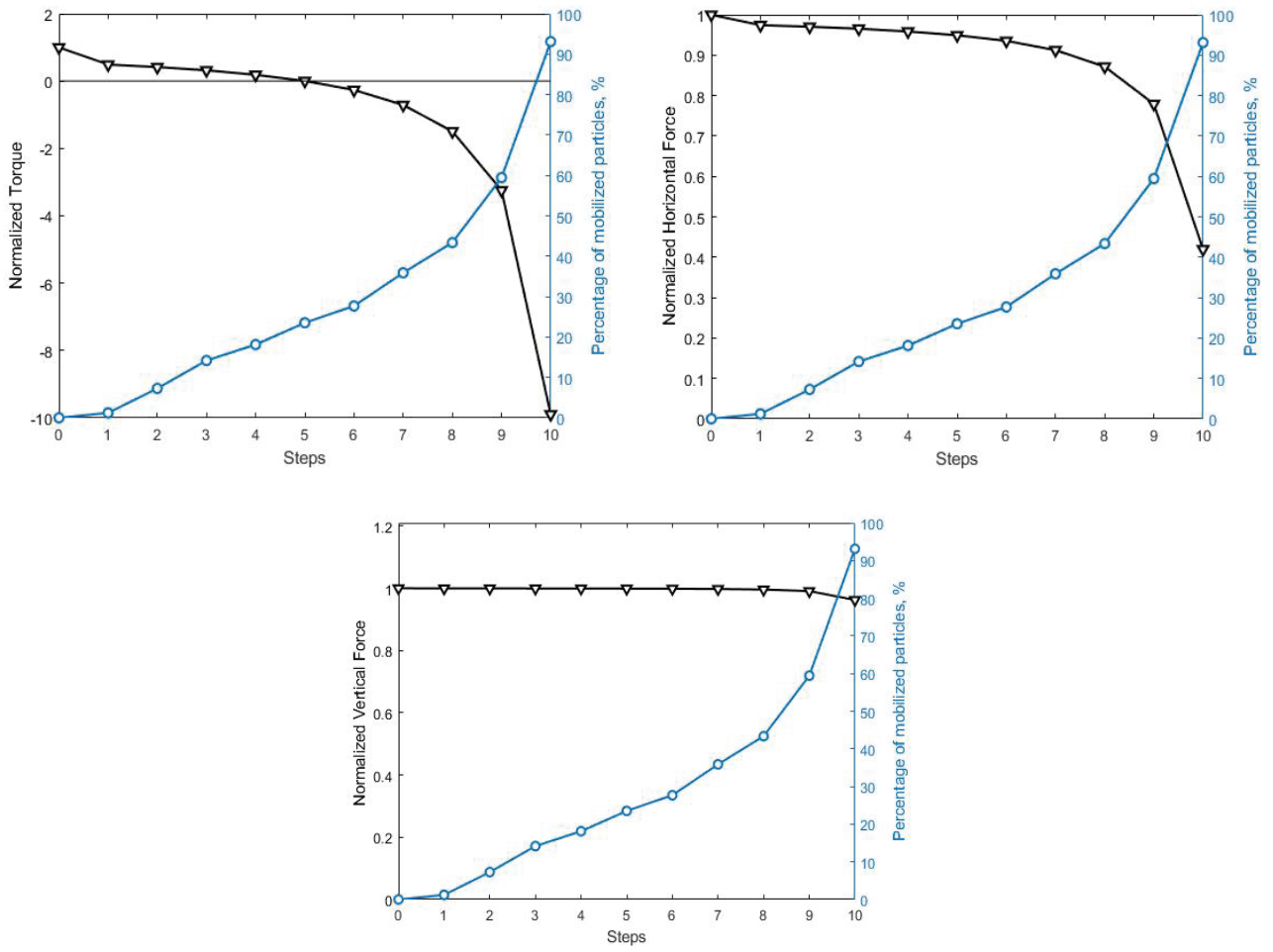

Figure 7: Condition of mechanical equilibrium for unfavorable attachment (Test 2): a) Normalised rolling torque; b) Normalised horizontal force; c) Normalised vertical force.

substrate surface. The gradual detachment is explained by particle distribution over radius. The mechanical equilibrium conditions as calculated based on average particle radius, qualitatively reflects detachment of the particles larger than the average size, while the smaller particles remain attached. This allows claiming qualitative agreement of laboratory observations with the mathematical model. The above results correspond to fines detachment in both cases of favorable and unfavorable detachment.

First test has been performed under high salinity and low pH (0.3M, pH3), while the second test was performed under low salinity and high pH (0.1M, pH9).Therefore, the first test exhibits high electrostatic attraction corresponding to deep single primary energy minimum. To the contrary, weak electrostatic attraction causes two energy minima with the shallow secondary minimum. Strong electrostatic attraction causes no particles detachment by lifting force (figure 6c), while weak attraction results in lifting of significant fraction of particles (figure 7c.)

More intensive detachment of particles under unfavorable conditions is attributed to shallow secondary energy minimum. The particles remaining attached at the end of Test 2 are located in primary minimum.

Acknowledgement

The authors are grateful to Dr. L. Chequer and Engs. M. Naby and M. Hussaini for support and fruitful discussions.

References

1. Vasiliadou IA, Chrysikopoulos CV (2011) Cotransport of Pseudomonas putida and kaolinite particles through water-saturated columns packed with glass beads. Water Resour Res 47.
2. Song W, Kovscek AR (2015) Functionalization of micromodels with kaolinite for investigation of low salinity oil-recovery processes. Lab Chip 15: 3314-3325.
3. Won J, Choo H, Burns SE (2020) Impact of Solution Chemistry on Deposition and Breakthrough Behaviors of Kaolinite in Silica Sand. J Geotech Geoenviron 146.
4. Chrysikopoulos CV, Aravantinou AF (2014) Virus attachment onto quartz sand: Role of grain size and temperature. J Environ Chem Eng 2: 796-801.
5. Bradford SA, Torkzaban S, Shapiro A (2013) A theoretical analysis of colloid attachment and straining in chemically heterogeneous porous media. Langmuir 29: 6944-6952.

6. Bradford SA, Torkzaban S, Wiegmann A (2011) Pore-scale simulations to determine the applied hydrodynamic torque and colloid immobilization. Vadose Zone J 10: 252-261.

7. Shen CY, Bradford SA, Li T, Li B, Huang Y (2018) Can nanoscale surface charge heterogeneity really explain colloid detachment from primary minima upon reduction of solution ionic strength? J Nanopart Res 20: 165.

8. Tosco T, Tiraferri A, Sethi R (2009) Ionic strength dependent transport of microparticles in saturated porous media: Modeling mobilization and immobilization phenomena under transient chemical conditions. Environ Sci Technol 43: 4425-4431.

9. Brady PV, Cygan RT, Nagy KL (1996) Molecular controls on kaolinite surface charge. J Colloid Interface Sci 183: 356-364.

10. Fountouli TV, Chrysikopoulos CV, Tsanis IK (2019) Effect of salinity on formaldehyde interaction with quartz sand and kaolinite colloid particles: batch and column experiments. Environ Earth Sci 78: 152.

11. Russell T, Pham D, Neishaboor MT, Badalyan A, Behr A, et al. (2017) Effects of kaolinite in rocks on fines migration, J Natural Gas Sci Eng 45: 243-255.

12. Bergendahl J, Grasso D (2000) Prediction of colloid detachment in a model porous media: hydrodynamics. Chem Eng Sci 55: 1523-1532.

13. Bedrikovetsky P, Siqueira FD, Furtado CA, de Souza ALS (2011) Modified particle detachment model for colloidal transport in porous media. Transp Porous Media 86: 353-383.

14. Bedrikovetsky P, Zeinijahromi A, Siqueira FD, Furtado CA, de Souza ALS (2012) Particle detachment under velocity alternation during suspension transport in porous media, Transp Porous Media 91: 173-197.

15. Yuan H, Shapiro AA (2011) Induced migration of fines during waterflooding in communicating layer-cake reservoirs. J Petrol Sci Eng 78: 618-626.

16. Yuan H, Shapiro AA (2011) A mathematical model for non-monotonic deposition profiles in deep bed filtration systems. Chem Eng J 166: 105-115.

17. Yang Y, Siqueira FD, Vaz ASL, You Z, Bedrikovetsky P (2016) Slow migration of detached fine particles over rock surface in porous media. J Nat Gas Sci Eng 34: 1159-1173.

18. Russell T, Bedrikovetsky P (2018) Colloidal-suspension flows with delayed fines detachment: Analytical model & laboratory study. Chem Eng Sci 190: 98-109.

19. Yuan B, Moghanloo RG (2017) Analytical model of well injectivity improvement using nanofluid preflush. Fuel 202: 380-394.

20. Yuan B, Moghanloo RG, Zheng D (2016) Analytical evaluation of nanoparticle application to mitigate fines migration in porous media. SPE Journal 21: 2,317-312,332.

21. Chequer L, Bedrikovetsky P (2019) Suspension-colloidal flow accompanied by detachment of oversaturated and undersaturated fines in porous media. Chem Eng Sci 198: 16-32.

22. Elimelech M, Gregory J, Jia X (1995) Particle Deposition and Aggregation 1st Edition: Measurement, Modelling and Simulation: Butterworth-Heinemann.

23. Derjaguin BV, Muller VM, Toporov YP (1975) Effect of contact deformations on the adhesion of particles. J Colloid Interface Sci 53: 314-326.

24. Chequer L, Carageorgos T, Naby M, Hussaini M, Lee W, et al. (2021) Colloidal detachment from solid surfaces: phase diagrams to determine the detachment regime. Chem Eng Sci 229: 116146.

25. Bedrikovetsky P (1993) Mathematical theory of oil and gas recovery (with applications to ex-USSR oil and gas fields) (Volume 4). Springer Science & Business Media: 576.

26. Kalantariasl A, Bedrikovetsky P (2013) Stabilization of external filter cake by colloidal forces in a "well–reservoir" system. Ind Eng Chem Res 53: 930-944.

27. Kalantariasl A, Zeinijahromi A, Bedrikovetsky (2014) Axi-symmetric two-phase suspension-colloidal flow in porous media during water injection. Ind Eng Chem Res 53: 15763-15775.

28. Kanimozhi B, Rajkumar P, Kumar RS, Mahalingam S, Thamizhmani V, et al. (2021) Kaolinite fines colloidal-suspension transport in high temperature porous subsurface aqueous environment: Implications to the geothermal sandstone and hot sedimentary aquifer reservoirs permeability. Geothermics 89: 101975.

29. Ramandi HL, Pirzada MA, Saydam S, Arns C, Roshan H (2021) Digital and experimental rock analysis of proppant injection into naturally fractured coal. Fuel 286: 119368.

30. Khuzhayorov BK, Makhmudov JM, Fayziev BM, Begmatov TI (2020) Some Model of a Suspension Filtration in a Porous Media That Accounts for the Two-Zone and Multistage Character of Deposition Kinetics. J Soc Ind Appl 14: 513-523.

31. Boccardo G, Tosco T, Fujisaki A, Messina F, Raoof A, et al. (2020) A review of transport of nanoparticles in porous media: From pore- to macroscale using computational methods. Nanomaterials for the Detection and Removal of Wastewater Pollutants 351-381.

32. Yosri A, Dickson-Anderson S, El-Dakhakhni W (2020) A Modified Time Domain Random Walk Approach for Simulating Colloid Behavior in Fractures: Method Development and Verification. Water Resour Res 56: e2020WR027599.